Simulation of rail yard emissions transport to the near-source environment

Gayle S.W. Hagler[a,*], Wei Tang[b]

[a]US EPA, Office of Research and Development, National Risk Management Research Laboratory, Research Triangle Park, NC, USA

[b]Lockheed Martin Corporation, Information Systems & Global Services, Durham, NC, USA

Abstract

Rail yards are critical nodes in the freight transportation network and locations of clustered emission sources. When people reside in close proximity to an active rail yard, the near-field effect of rail yard emissions is of concern. Field characterization of near-rail yard air quality is challenging due to spatially-variable emissions over a large area. Numerical models can provide valuable insight into factors affecting emission dispersion and resulting near-field air pollution. This study utilizes computational fluid dynamics (CFD) modeling to investigate near-field air pollution surrounding a generic, moderate-sized intermodal rail yard with emissions of a neutrally buoyant gaseous pollutant. Rail yard and surrounding neighborhood structures were added in succession to a base case to study the influence of surface roughness on the generic pollutant's spatial concentration profile. A spatially weighted emissions scenario reveals highly variable pollutant levels in downwind neighborhoods, strongly modulated by wind direction. Rail yard topography (containers, cranes, small buildings) was found to result in a modest increase in near-field pollution levels. Densely located two-story homes surrounding the rail yard reduced downwind concentrations by 16% and 15% at 25 m and 100 m downwind of the rail yard boundary, respectively. Adding a 6 m boundary wall to the rail yard, with four open sections in the wall enabling traffic flow, leads to a reduction in downwind pollution levels by 25% and 12% at 25 m and 100 m downwind, respectively. While area-wide pollution levels are reduced with the addition of neighborhoods and a surrounding boundary wall, high spatial variability in pollution levels in the near-field area lead to some areas with increased pollution levels offset by a reduction in pollution in other near-field areas. Overall, these findings suggest that pollution levels in the near-rail yard area have a high degree of spatial variability, with topographical elements surrounding the

rail yard (neighborhood structures, boundary wall) resulting in a net effect of near-field pollution reduction.

1. Introduction

Air pollution in close proximity to major transportation sources – such as a highway, rail yard, or port – has been an issue of increasing concern in the public consciousness. A significant number of studies have found repeatable evidence of elevated air pollution in close proximity to major highways (Karner et al., 2010 and references therein) and a recent synthesis of health studies indicated adverse health effects associated with proximity to a major roadway (HEI Panel on the Health Effects of Traffic-Related Air Pollution, 2010). Comparatively fewer studies have measured local air pollution trends related to other major transportation facilities, such as ports, rail yards, intermodal facilities, and airports. Understanding air pollution related to freight transportation is an ongoing topic of concern, with an increasing interest in higher-spatial resolution analyses to understand microenvironments, local scale (hundreds of meters), and regional-scale (tens of kilometers) air pollution trends and effects of changing source emissions (Bickford et al., 2014; Hagler et al., 2013; Joe et al., 2014).

Rail yards, the primary focus of this study, are complex environments with a variety of emission sources distributed over a large area. Sources vary from one rail yard to another – classification rail yards move freight between trains and therefore have primarily locomotive and container-handling equipment emissions, and intermodal rail yards additionally have truck traffic transporting freight to and from the rail yard. In addition to the heterogeneous rail yard emissions, the surrounding environment can add further complexity; other major sources in close proximity (e.g., manufacturing, highways) and the built environment can impose additional variability on local air pollution. Project-based risk assessments have been conducted using regulatory models for numerous rail yards in the United States based upon state requirements (e.g., Health Risk Assessments in California available at http://www.arb.ca.gov/railyard/hra/hra.htm). Field characterization of local air quality near rail yards has been conducted at only a handful of locations in the United States. Local-scale effects of rail yard emissions were quantified at a major classification rail yard in California (Cahill et al., 2011), a moderate-sized intermodal facility in Illinois (Rizzo et al., 2014), and two adjacent intermodal rail yards in Georgia (Galvis et al., 2013). Collecting representative field data can be challenging given local meteorology and the higher likelihood of confounding sources nearby in industrial areas. For example, while a model of an intermodal rail yard in Michigan was found to locally impact fine particulate matter concentrations ($PM_{2.5}$, particulate mass smaller than 2.5 μm) (Turner, 2009), major facilities in close proximity to the rail yard confounded field characterization of local air pollution.

Given the complexity of resolving local air pollution trends related to rail yard emissions, high resolution models complement field characterization through simulating the distribution of pollutant concentrations in the near-field environment and isolating influential factors. Computational fluid dynamics (CFD) modeling is one approach that supports a very fine-grained assessment of emissions transport in a complex environment. For example, CFD simulations can be used to investigate how surrounding neighborhood buildings may alter the near-rail yard concentrations and whether a boundary wall would improve or degrade local air quality. To date, the application of CFD for rail yard environments has been primarily utilized for emergency release analyses, such as evaluating the dispersion of an accidental release of dense chlorine gas (e.g., Hanna et al., 2009). This present study focuses on estimating effects of rail yard emissions related to freight movement and uses a neutrally buoyant tracer that would be more representative of common gaseous air pollutants emitted from combustion. This study utilizes CFD modeling to simulate a rail yard environment and understand the effect of emissions location, rail yard, surrounding topography, and wind direction on predicted pollutant concentrations. The research approach balances the desire for a realistic simulation with a goal of providing generalizable findings, utilizing a published emissions inventory to inform emissions weighting, and an existing rail yard to guide the physical dimensions and topography.

2. Methods

2.1 Model geometry

A series of 3-dimensional computer models of an idealized rail yard were constructed to be similar in scale to a moderate-sized intermodal rail yard in Illinois studied by Rizzo et al. (2014). Five surface scenarios were developed with incrementally added terrain features (Table 1) including, (1) base model with uniformly distributed source elements; (2) base model with rail containers, buildings, and cranes added; (3) addition of a surrounding boundary wall to scenario (2); (4) addition of surrounding neighborhood buildings to scenario (2); and, (5) addition of surrounding neighborhood buildings to scenario (3).

As shown in Figure 1, the simulated rail yard area resembled an oval spanning 2700 m along the rail track direction and 500 m across, i.e. length to width ratio of 5.4 to 1. A total of 2656 ground-placed source elements, each measured 2 m × 2 m × 4.5 m (L × W × H), were added with the center of each element's base plane located on a 20 m grid. The source elements were transparent to mean flow, i.e., they don't obstruct flow but serve as sources of turbulence and emission of an inert gaseous tracer with the same density as air during the CFD simulations. The source strength of each element can be adjusted individually. This approach allows flexibility in simulating various emission scenarios, such as homogeneous emissions across the rail yard, or higher emissions along the main rail track and certain high locomotive activity areas. The 3D computational domain measured 3700 m × 1500 m × 200 m, which extended 500 m outside the rail yard.

Terrain elements observed in a typical rail yard, including rail containers, buildings and cranes, were added to the base model to study their influence on pollutant transport. All containers were 12.5 m long by 2.5 m wide by 2.5 m high. There were 146 containers along the main through rail track (shown in yellow), and 95 containers on each of the 7 parallel tracks spaced 20 m apart (shown in green). Three container parking areas were included (shown in teal): 2 arrays of 8 by 25 containers on either side of the tracks, and 1 array of 24 by 14 containers at the east end of the rail yard, oriented at a 45 degree angle. The added six buildings, modeled after typical 1-story storage structures, were 24 m wide by 10 m high, and either 36 m or 72 m long. Four cranes with dimensions of 6 m × 16 m × 14 m (L × W × H) were placed among the parallel train tracks.

To study the impact of a boundary barrier on near-rail yard air pollutant concentrations, a solid 0.5 m thick wall was added all around the rail yard. The wall had breaks at each end where the main train track passed through and one break on the NW side and one on the SW side. Four different wall heights were simulated: 3 m, 6 m, 9 m, and 18 m (0.5H, 1H, 1.5H, and 3H).

The final addition to the rail yard model was the surrounding neighborhood, which consisted of approximately 96 idealized residential blocks. Most blocks were 20 lots wide and 2 lots deep (200 m by 90 m), while a few blocks near either end of the rail yard were cropped to make room for the rail yard. All blocks were spaced 20 m apart. Within the blocks, each lot had a footprint of 40 m by 10 m and includes a two-story house in the front and a one-story garage/shed in the back. Their dimensions were 14 m × 8 m × 11.25 m and 8 m × 8 m × 7.5 m respectively.

2.2 Modeling approach

Volume meshes were constructed using the commercial software Harpoon (Sharc Ltd., Manchester, UK), which produces a body-fitted, hex-dominant mesh based on octree decomposition of the domain. Several tests, similar in approach as described in an earlier study of roadside barrier effects (Hagler et al., 2011), were performed to verify grid size independence with increasing number of mesh cells until further refinements produced no significant improvements. The final mesh had graduated cell sizes, ranging from 0.25 m in close proximity to the terrain elements and increasing with distance from the element surfaces to 8 m maximum. The overall mesh size ranged from 30 million for the base model, and up to 72 million for the model with boundary wall and neighborhood added.

Numerical simulations of rail yard emissions transport to the near-source environment were conducted using the CFD code FLUENT 12.0 (ANSYS, Inc). The modeling approach is similar to that of an earlier study of roadside barrier effects on near-road air quality (Hagler et al., 2011). A neutral atmospheric boundary layer was assumed for all simulations. The inlet boundary of the model was defined as a velocity inlet. Inlet profiles for mean velocity, turbulent kinetic energy (TKE), and ε (turbulent dissipation) were derived via a 2D case with periodic boundary condition that simulates a fully developed atmospheric boundary layer with a logarithmic profile, matching the mean velocity and TKE of the approach flow in a wind tunnel model (Heist et al., 2009). The incoming boundary layer had a roughness length of 0.36 m and a friction velocity of 0.25 m/s. The wind speed at 30 m from the ground was 3 m/s. A pressure outlet was specified at the downstream end of the domain. Symmetry conditions were imposed on the top and lateral sides of the domain. The ground was set as a wall condition with roughness z_0 = 0.05 m, which simulates a relatively smooth ground while the terrain elements and source volumes were responsible for most of the turbulence generated in the model.

Two types of source configurations were studied: homogeneous emissions and weighted emissions within the rail yard. We assumed a total emission rate of 50 ton per year of an inert gaseous tracer with the same density as air. For configuration 1, the emissions were evenly spread among all 2,656 source elements, while for configuration 2, the emissions were spatially weighted to represent a more realistic rail yard scenario. Based on a published intermodal rail yard emission inventory (Turner, 2009), the primary sources of a rail yard were line haul locomotives on the train tracks and switch locomotives that performed yard-specific operations. The former accounted for 43% of the total emissions, and the later accounted for 54% of the total emissions. The remaining 3% was other distributed non-locomotive emissions. To simulate such partitioning, source strength was significantly increased for 130 source elements along the main track and for 80 source elements on either end of the parallel tracks where the switch locomotives operated. The source strength of the other elements was reduced to make up for the remaining 3%.

The FLUENT code solves conservation equations for mass, momentum and energy. For turbulent flows, the Reynolds-averaged approach is employed to solve the Navier-Stokes equations. A number of turbulence models are provided in FLUENT to achieve closure (ANSYS, 2009). In this study, the Realizeable k-ε model (Shih et al., 1995) with a Schmidt number of 1.0 was selected based on comparison with wind tunnel data, as documented in the roadside barrier study (Hagler et al., 2011). Various models are available in FLUENT to simulate the mixing and transport of an airborne species. This study employed the advection diffusion (AD) module, which computes the diffusive mass flux of the species and satisfies the conservation of mass. All simulations used the implicit formulation, segregated and steady solvers. Standard discretization was used for the pressure terms. Second-order upwinding discretization schemes were used for momentum, turbulence, and species to increase accuracy and reduce numerical diffusion. The SIMPLE (Semi-Implicit Method for Pressure Linked Equations) algorithm was specified for pressure-velocity coupling to improve convergence. FLUENT uses an iterative method to solve the algebraic system of equations. The residuals for all field variables were closely monitored. Convergence was deemed achieved when all residuals approached an asymptote. The termination residual values were on the order of 10^{-5} to 10^{-7}. The simulations were performed on the EPA's high performance computing system Terra, an IBM iDataPlex cluster, using between 64 to 256 cores for different runs. The total simulation time ranged from 2200 CPU hours for the base case up to 10000 CPU hours for the model with terrain elements, boundary wall and neighborhood added. The wall-clock time was significantly shorter, never more than 72 hours.

Model results are primarily discussed in terms of normalized pollutant concentrations (χ), quantified as $\chi = CU_rL_xL_y/Q$, where C is the background-adjusted concentration, U_r is the reference wind speed measured at a full-scale equivalent of 30 m, L_x and L_y are the model dimensions, and Q is the tracer emissions rate. In addition, TKE is also discussed, which represents the kinetic energy of the air mass throughout the model domain. The various scenarios are referred to using a naming scheme described in Table 1.

3 Results and Discussion

3.1 Effect of rail yard interior topography and emissions weighting on downwind dispersion

In order to isolate the effect of individual features hypothesized to influence downwind dispersion of rail yard emissions – including within-yard structures, wind direction, and emissions locations – a homogenous area source (scenario B) was used as a starting point. Rail yard elements (containers, cranes, building structures) were added to this homogenous emissions environment (scenario B-Y), with a close view of the model displaying the location of structures with areas of open space (Figure 2) to approximate the density of structures observed in an aerial view of a mid-sized rail yard in Illinois, United States (Rizzo et al., 2014). The addition of these rail yard structures is observed to modestly alter the dispersion of the homogenous emissions field, with the difference between the base case

(Figure 3a) and base case with yard structures (Figure 3b) showing only slight difference in concentrations (Figure 3c).

Bringing the model closer to reality by spatially weighting the emissions (scenarios B-E, B-EY), much greater spatial variability is evident (Figure 4) and rail yard terrain structures in areas of higher emissions have more impact on downwind pollutant levels. In order to quantify the difference between scenarios, the mean and standard deviation of the normalized pollutant concentration (χ) is estimated at a set offset distance from the upper rail yard boundary and under 45 degree wind (air transported from the lower left to the upper right) and weighted emission scenarios (Table 2). For example, the addition of rail yard structures leads to a slightly increased and more variable χ overall, at distances of 25-400 m in distance from the rail yard boundary. While rail yard structures may enhance upward mixing and dilution, the terrain elements have a competing effect of slowing air flow and trapping air pollution near the point of emissions.

3.2 Wind direction effect

Given the oblong scale of the rail yard model, shifting the wind direction over a 90-degree range led to significant change in the location and level of simulated downwind pollution. With winds parallel to the rail yard (Figure 5, 0 degree scenario), maximum concentrations occurred in the downwind area of the rail yard closest to the location of the simulated train tracks. For scenario B-EY, χ values reached ~100 in a small spatial area and very low concentrations (χ ranging 0-10) occurred in other near-rail yard areas. For scenario B-Y, maximum local χ values near the rail yard were apparent under the 0 degree winds. Meanwhile, for the weighted emissions scenario (B-EY), oblique winds (Figure 5, 45 degree case) led to a large spatial region of high χ values (~100). These scenarios illustrated the challenge in characterizing rail yard environments or similar large area sources of heterogeneous emissions, where pollutant levels were anticipated to have high spatial and temporal variability under changing winds and emissions strengths.

3.3 Influence of surrounding neighborhood buildings

The occurrence of neighborhood structures surrounding a rail yard may affect the overall air flow entering the rail yard and downwind dispersion of emissions. The rail yard model configuration added a dense network of single-family residential buildings with detached garage units that approximate the neighborhoods surrounding a rail yard selected in Cicero, Illinois (Figure 1 and 2). Comparing the scenario with weighted emissions and rail yard structures (B-EY), with and without surrounding neighborhoods, the majority of the downwind area experiences χ decreases, particularly in areas with higher baseline concentrations (Figure 6). Modest increases are also observed in several areas, with the simultaneous existence of increases and decreases likely due to the added structures inducing competing effects of increased vertical dispersion and local trapping of emissions. Overall, the addition of neighborhoods is estimated to reduce concentrations at 25 m and at 100 m from the rail yard boundary by approximately 16% and 15%, respectively (Table 2). This net decrease agrees with the modestly higher normalized TKE shown within and surrounding the rail yard, due to the addition of neighborhood structures (Figure S1, case B-EYN).

3.4 Boundary wall effect

Noise walls have been a subject of interest in recent years for their potential to reduce traffic-related air pollution nearby major roadways (Baldauf et al., 2008; Hagler et al., 2011) by increasing vertical dispersion of emissions. For a rail yard environment, a boundary wall could conceivably be employed as a mitigation approach, with points of opening for rail lines and truck traffic. In model scenario B-EYW, a 6 m solid boundary wall was placed surrounding the yard, with four breaks in the wall allowing for rail lines and/or trucks to pass through. Subtracting the identical scenario without a wall (B-EY), it can be observed that significant reductions in concentrations (e.g., net χ = -25 to -75) occur with the wall present for portions of the yard that originally had high downwind concentrations with weighted emissions (Figure 7). However, net χ increases are also evident inareas downwind of a break in the wall and in areas downwind of a combination of the wall plus a larger building in the yard. Overall, the scenarios involving a boundary wall (B-EYW, B-EYWN) all had lower mean χ values downwind of the rail yard (Table 2). Comparing the two scenarios with weighted emissions, yard structures, and surrounding neighborhood buildings, the mean χ with the wall was 25% lower at 25 m and 12% lower at 100 m. This reduction is likely due to increased vertical mixing, as normalized TKE is observed to increase downwind of the wall (Figure S1, case B-EYWN and B-EYW).

4 Conclusion

Assessing air pollution surrounding large facilities with spatially heterogeneous emissions is challenging to accomplish in field settings. Rail yards in densely populated areas are particularly complex to study, typically a geographically large and heterogeneous emissions environment surrounded by a dense building configuration. High resolution models, even generic ones, can provide insight into the multiple factors affecting emissions transport to the near-field environment. In this present study, multiple parameters were explored that were hypothesized to influence rail yard emissions transport and resulting downwind pollution levels. Simulating a generic mid-sized rail yard environment, maximum near-field concentrations occurred under a simple model consisting of only spatially weighted emissions and typical structures within the rail yard (buildings, containers). Including neighborhood buildings and a surrounding boundary wall both independently resulted in lower mean concentrations in the near-field environment. Looking beyond average concentrations, the model simulations also demonstrate highly variable pollution levels and indicate high concentration zones directly downwind of concentrated emissions areas. It is important to note that these results are limited in simulating a neutrally buoyant tracer gas, and therefore may not represent pollutants of differing physicochemical properties. In addition, the findings do not represent the full variety of local meteorological conditions that would be experienced within a typical year. Despite these limitations, the model results help isolate and quantify the effects of different factors impacting near-field air pollution. These findings are anticipated to support field data interpretation, such as analysis of mobile monitoring data collected along roadway networks near a rail yard (e.g., Rizzo et al., 2014).

References.

ANSYS, Inc., 2009. FLUENT 12.0 User’s Guide.

Baldauf, R. et al., 2008. Impacts of noise barriers on near-road air quality. Atmospheric Environment, 42(32): 7502-7507.

Bickford, E. et al., 2014. Emissions and Air Quality Impacts of Truck-to-Rail Freight Modal Shifts in the Midwestern United States. Environmental Science & Technology, 48(1): 446-454.

Cahill, T.A., Cahill, T.M., Barnes, D.E., Spada, N.J., Miller, R., 2011. Inorganic and organic aerosols downwind of California's Roseville railyard. Aerosol Science and Technology, 45(9): 1049-1059.

Galvis, B., Bergin, M., Russell, A., 2013. Fuel-based fine particulate and black carbon emission factors from a railyard area in Atlanta. Journal of the Air & Waste Management Association, 63(6): 648-658.

Hagler, G.S.W. et al., 2013. Panama Canal Expansion Illustrates Need for Multimodal Near-Source Air Quality Assessment. Environmental Science & Technology, 47(18): 10102-10103.

Hagler, G.S.W. et al., 2011. Model evaluation of roadside barrier impact on near-road air pollution. Atmospheric Environment, 45(15): 2522-2530.

Hanna, S.R., Hansen, O.R., Ichard, M., Strimaitis, D., 2009. CFD model simulation of dispersion from chlorine railcar releases in industrial and urban areas. Atmospheric Environment, 43(2): 262-270.

HEI Panel on the Health Effects of Traffic-Related Air Pollution, 2010. Traffic-Related Air Pollution: A Critical Review of the Literature on Emissions, Exposure, and Health Effects, Health Effects Institute. Boston, Mass. Web-available at: http://pubs.healtheffects.org/getfile.php?u=553 (accessed on August, 2015)

Heist, D.K., Perry, S.G., Brixey, L.A., 2009. A wind tunnel study of the effect of roadway configurations on the dispersion of traffic-related pollution. Atmospheric Environment, 43(32): 5101-5111.

Joe, D.K. et al., 2014. Implementation of a high-resolution Source-Oriented WRF/Chem model at the Port of Oakland. Atmospheric Environment, 82: 351-363.

Karner, A.A., Eisinger, D.S., Niemeier, D.A., 2010. Near-Roadway Air Quality: Synthesizing the Findings from Real-World Data. Environmental Science & Technology, 44(14): 5334-5344.

Rizzo, M. et al., 2014. Cicero Rail Yard Study (CIRYS) Final Report, EPA /600/R/12/621. Available by web at: http://nepis.epa.gov/Adobe/PDF/P100IVT3.pdf (Accessed on August 2015)

Shih, T.H., Liou, W.W., Shabbir, A., Yang, Z., Zhu, J. A New k-ε Eddy Viscosity Model for High Reynolds Number Turbulent Flows—Model Development and Validation. Computers Fluids. 24(3):227-238, 1995

Turner, J.R., Yadav, V., and Feinberg, S.N., 2009. Data analysis and dispersion modeling of the Midwest rail study (Phase I) – final report, http://www.ladco.org/reports/general/new_docs/WUSTL_MidwestRailStudy_FinalReport.pdf.

Table 1. Description of rail yard modeling scenarios

Scenario	Spatially weighted emissions (E)	Rail yard structures (Y)	Surrounding boundary wall (W)	Surrounding houses (N)
Base (B)				
B-E	●			
B-Y		●		
B-EY	●	●		
B-EYW	●	●	●	
B-YW		●	●	
B-EYN	●	●		●
B-EYWN	●	●	●	●

Table 2. Concentrations at discrete distances for the weighted emissions scenarios and wind at 45 degrees.[1]

	D = 25 m		D = 50 m		D = 100 m		D = 200 m		D = 400 m	
Scenario	**Mean**	**Std. dev.**	**Mean**	**Std. dev.**	**Mean**	**Std. dev.**	**Mean**	**Std. dev.**	**Mean**	**Std. dev.**
B-E	26.65	24.58	23.39	22.49	18.56	19.25	12.63	14.70	7.16	9.70
B-EY	29.39	27.40	25.28	24.55	19.70	20.73	13.29	15.76	7.51	10.35
B-EYW	20.46	17.87	20.20	17.56	16.39	15.69	11.35	12.17	6.74	8.44
B-EYN	25.36	23.53	23.28	22.36	17.13	17.19	12.21	13.82	7.15	8.92
B-EYWN	19.11	16.51	18.32	17.21	15.05	14.84	11.36	12.61	6.87	8.45

[1]Concentrations are estimated at a height of Z = 1.5 m and sampled as discrete points along a curved path offset by the rail yard by the set distance. The calculation excludes the lower half of the model space, which is upwind of the yard for the 45 degree and 90 degree wind case.

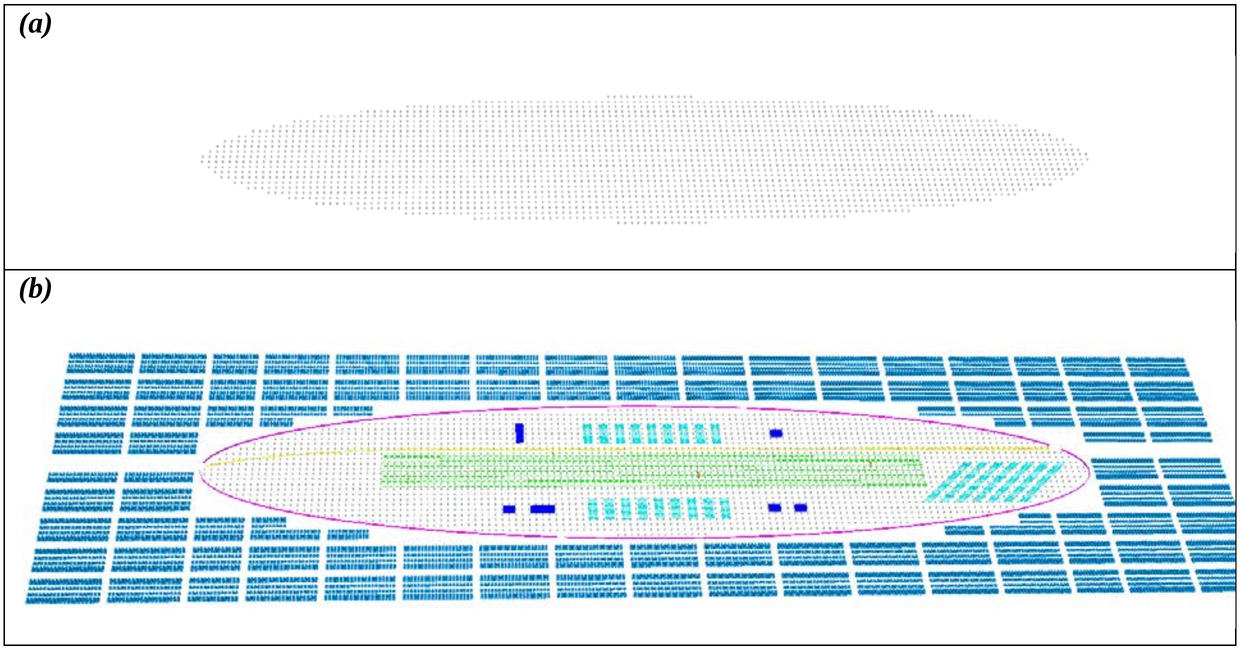

Figure 1. Model set-up from the simplified case of homogenous emissions distributed over an area (a) to the most complex case involving structures within the rail yard representing buildings and containers, a surrounding boundary wall, spatially-weighted emissions, and surrounding city blocks of residential buildings.

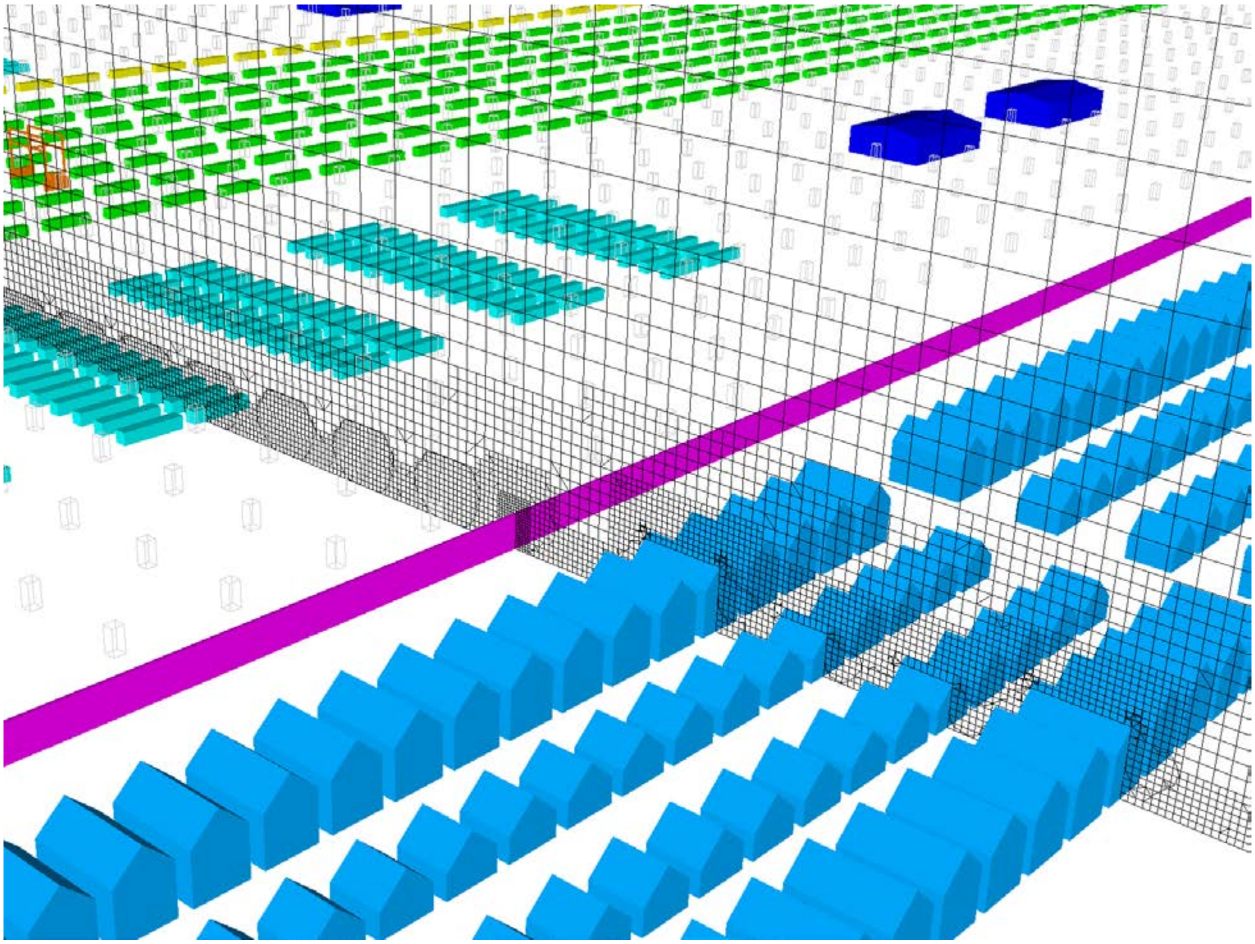

Figure 2. A zoom-in showing the structures and mesh on a Y-plane.

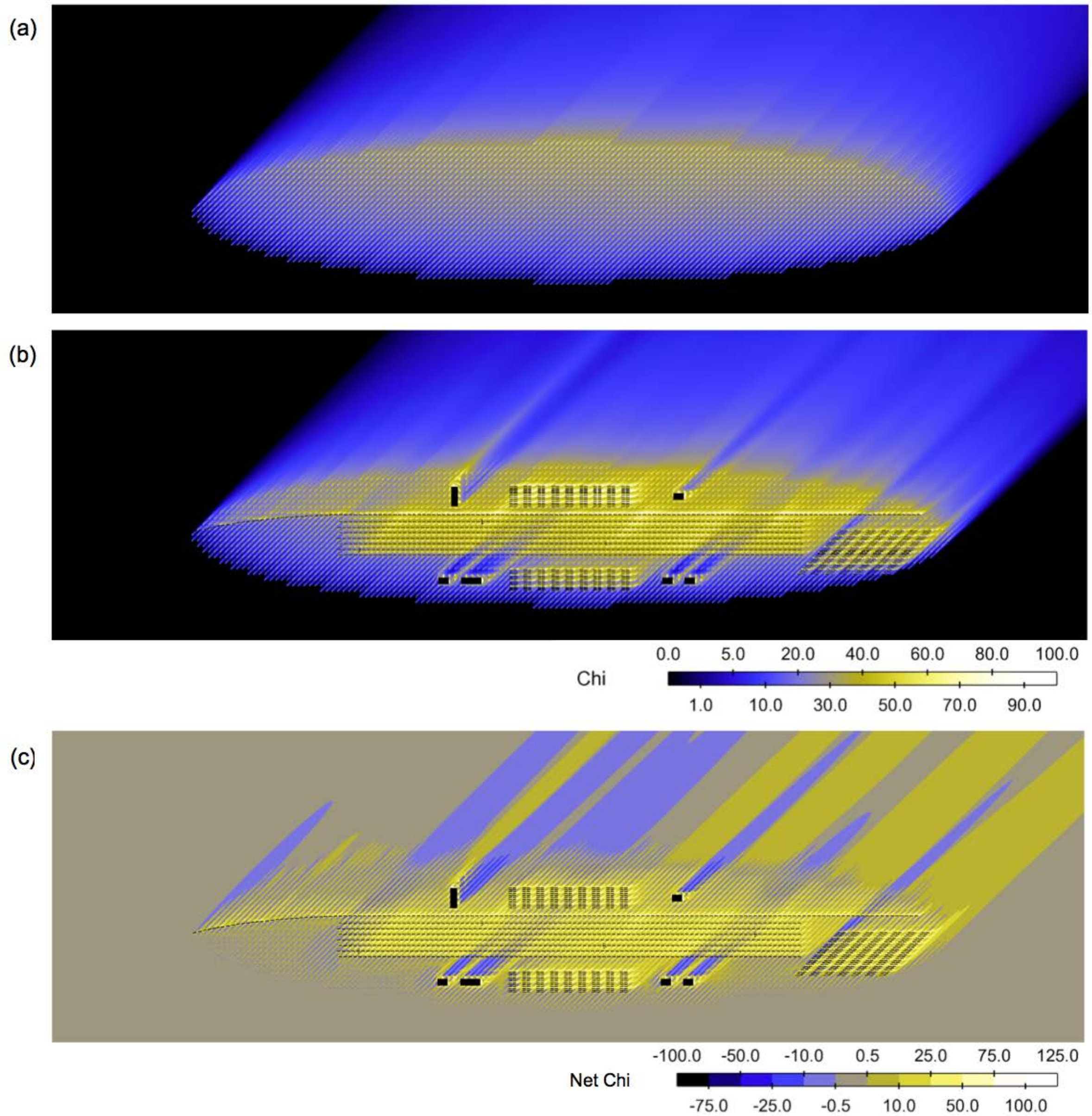

Figure 3. Concentration calculated at a height of 1.5 m for a) Scenario B, b) Scenario B-Y, c) Net χ = Scenario B-Y minus Scenario B, calculated at a height of 1.5 m.

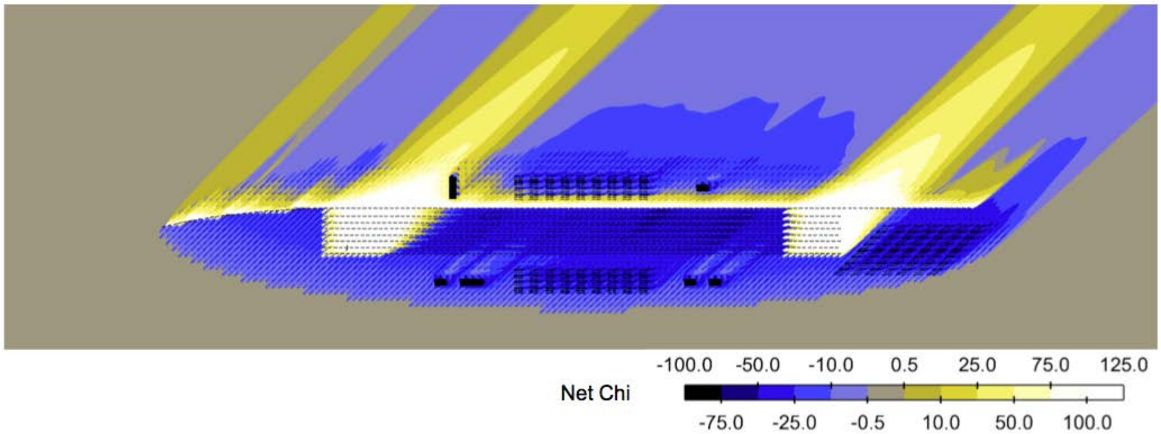

Figure 4. Difference in normalized pollutant concentrations with weighted versus unweighted emissions, in both cases with identical rail yard structures present. Net χ = Scenario B-EY minus Scenario B-Y, evaluated at a height of 1.5 m.

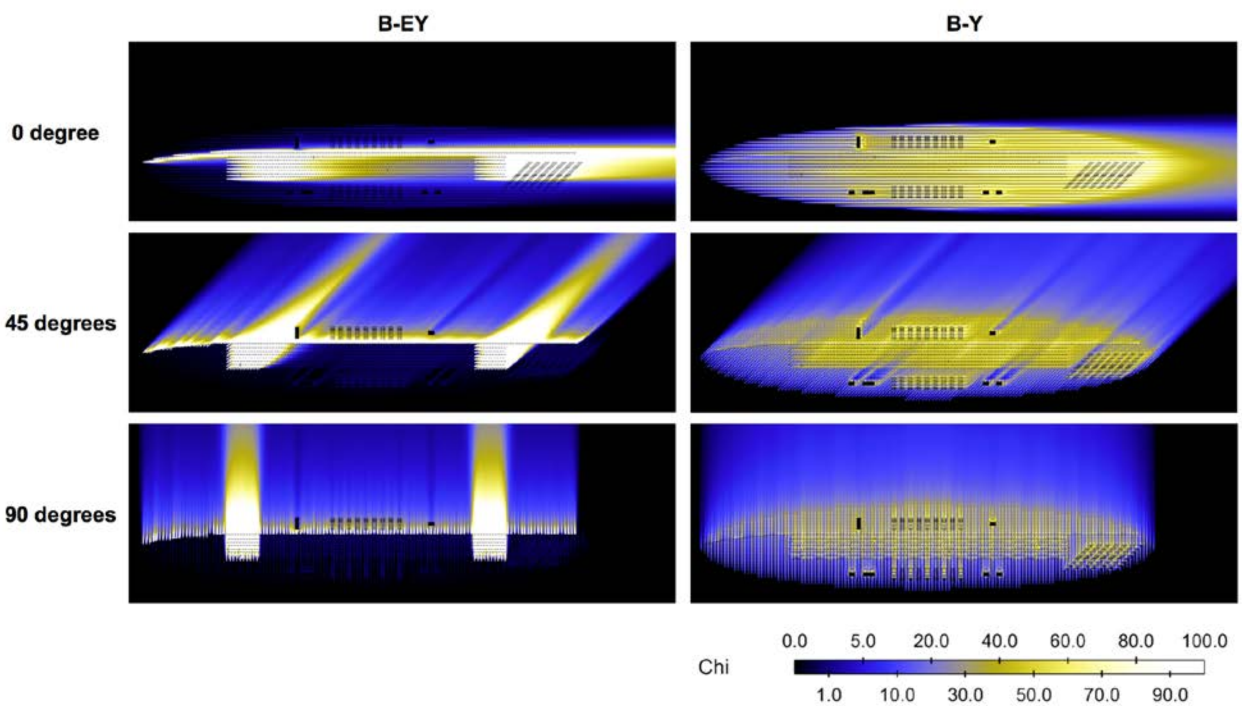

Figure 5. Spatial distribution of normalized pollution (χ) for Scenarios B-EY and Scenarios B-Y, with wind direction.

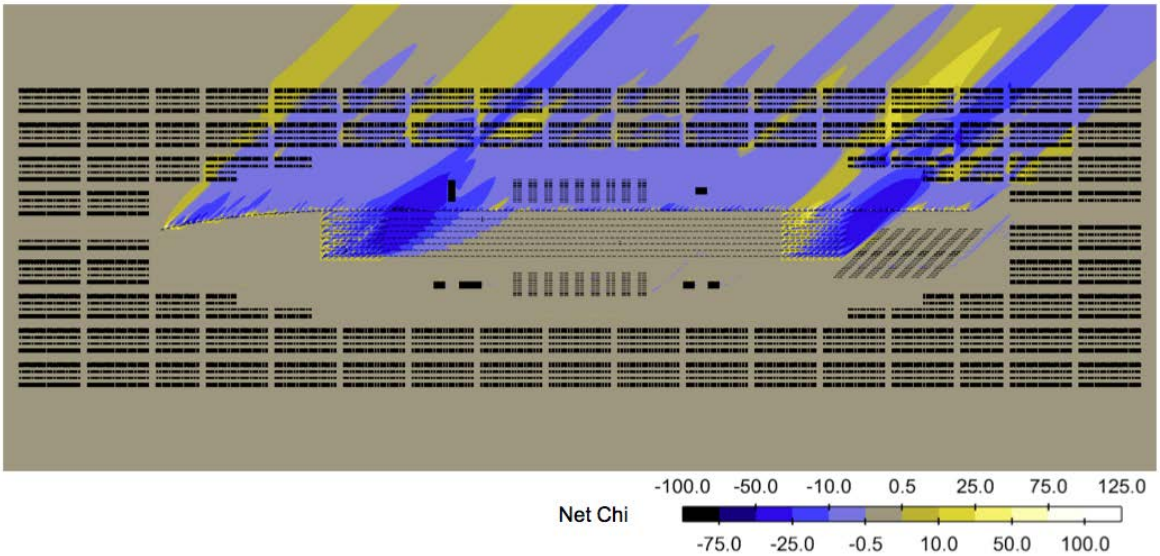

Figure 6. Difference in normalized pollutant concentrations with and without of neighborhood buildings, with both scenarios having weighted emissions and rail yard structures present. (Net χ = Scenario B-EYN minus Scenario B-EY).

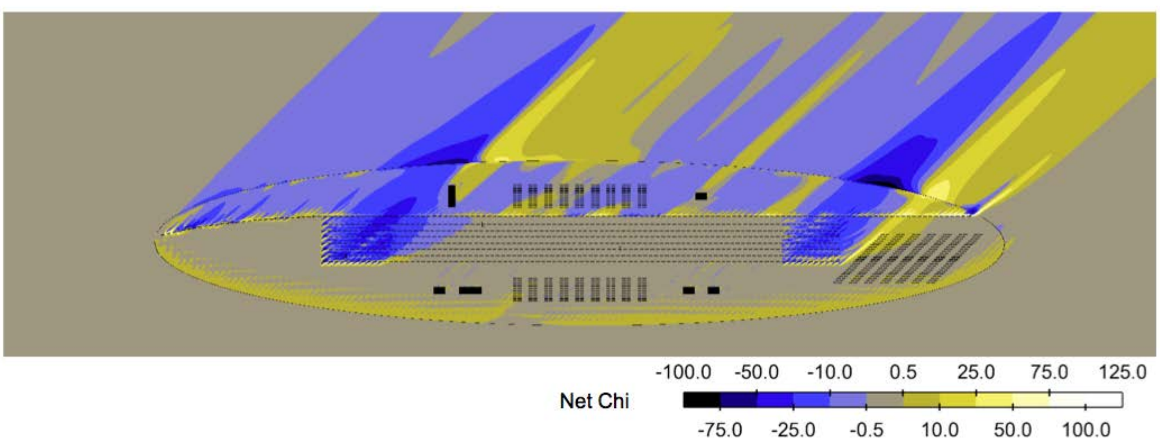

Figure 7. Difference in normalized pollutant concentrations with and without a 6 m boundary wall, with both scenarios having weighted emissions and rail yard structures present (Net χ = Scenario B-EYW minus Scenario B-EY).